Genetic evidence that SOST inhibits WNT signaling in the limb

Nicole M. Collette [a,b], Damian C. Genetos [c], Deepa Murugesh [a,b], Richard M. Harland [b], Gabriela G. Loots [a,b,*]

[a] Biology and Biotechnology Division, Lawrence Livermore National Laboratory, 7000 East Avenue, L-452, Livermore, CA 94550, USA
[b] Department of Molecular and Cell Biology, Division of Genetics, Genomics, and Development, and Center for Integrative Genomics, University of California, Berkeley, CA 94720-3204, USA
[c] Department of Surgical and Radiological Sciences, School of Veterinary Medicine, University of California, Davis, CA 95616, USA

ARTICLE INFO

ABSTRACT

SOST is a negative regulator of bone formation, and mutations in human *SOST* are responsible for sclerosteosis. In addition to high bone mass, sclerosteosis patients occasionally display hand defects, suggesting that *SOST* may function embryonically. Here we report that overexpression of *SOST* leads to loss of posterior structures of the zeugopod and autopod by perturbing anterior–posterior and proximal–distal signaling centers in the developing limb. Mutant mice that overexpress *SOST* in combination with *Grem1 and Lrp6* mutations display more severe limb defects than single mutants alone, while *Sost*$^{-/-}$ significantly rescues the *Lrp6*$^{-/-}$ skeletal phenotype, signifying that *SOST* gain-of-function impairs limb patterning by inhibiting the WNT signaling through LRP5/6.

© 2010 Elsevier Inc. All rights reserved.

Introduction

Sclerosteosis is an autosomal recessive form of generalized hyperostosis (MIM 239100) due to hyperactive osteoblast activity that results from loss of sclerostin or SOST expression. Targeted deletion of *Sost* in mice causes increased bone formation and bone strength, and administration of anti-sclerostin antibodies increases bone formation and restores bone loss in osteoporotic rats (Li et al., 2008a,b). For a minority of sclerosteosis patients, syndactyly of digits (Cremin, 1979) has been described primarily as asymmetric cutaneous syndactyly of the index and middle fingers (digits 2 and 3). Furthermore, some patients have remarkably deformed fingers with hypoplasia and nail dysplasia (symmetric or asymmetric) most commonly associated with the index finger (Cremin, 1979). We have previously reported that elevated levels of human *SOST* in transgenic mice cause a decrease in bone and mineral density in the appendicular and axial skeleton. We also noted that these mice display varying degrees of digit abnormalities ranging from fused and split to missing digits (Loots et al., 2005). While originally *SOST* was thought to primarily function in the adult skeleton as an osteocyte-secreted factor that negatively regulates bone formation (Balemans et al., 2001; Brunkow et al., 2001; Li et al., 2008a; van Bezooijen et al., 2004) and promotes osteoblast apoptosis (Sutherland et al., 2004), the hand abnormalities described for sclerosteosis patients along with the gain-of-function limb defects suggest that *SOST* may also function embryonically, during limb and hand formation.

Based on sequence similarity, SOST was originally identified as a member of the DAN family of cysteine-rich BMP antagonists that include DAN, Cerberus, GREM1, DAND5 (also known as CERL2, DANTE, COCO) and its paralog SOSTDC1 (also known as ectodin, SostL, USAG-1 and Wise) (Brunkow et al., 2001; Yanagita, 2005). While BMP2, 4, and 7 are largely dispensable for limb patterning (Bandyopadhyay et al., 2006), exogenous BMPs have been shown to affect the size and shape of long bones by increasing the recruitment of progenitor mesenchymal stem cells into the chondrogenic lineage (Duprez et al., 1996; Macias et al., 1997). However, both noggin and gremlin, which encode antagonists of BMP signaling, are essential for proper skeletal patterning (Benazet et al., 2009; Brunet et al., 1998; Khokha et al., 2003).

Similarly, WNT signal transduction is essential for limb development (Holmen et al., 2004; Pinson et al., 2000). Several WNTs have been shown to control early events during proximal–distal outgrowth and dorsoventral limb patterning as well as participate in later events during chondrogenesis, osteogenesis, muscle development, and joint formation. Mutations in human *WNT3* and *WNT7A* result in severe skeletal malformations (Niemann et al., 2004; Woods et al., 2006), and several mouse lines have been described where misregulation of WNT signaling causes limb defects (Galceran et al., 1999; Parr and McMahon, 1995). Like BMP signaling, WNT signaling is also attenuated at the receptor level by two types of regulatory proteins. Secreted frizzled related proteins (SFRP) directly bind to WNT ligands and prevent them from binding to the receptor, while members of the Dickkopf family (DKK) interact with the two WNT coreceptors, low-density lipoprotein receptor-related proteins 5 and 6 (LRP5/6) (Niehrs, 2006; Pinzone et al., 2009). The balance between ligands and antagonists modulate the inputs of WNT signaling and subsequently contribute to proper limb outgrowth, patterning, and cartilage differentiation.

* Corresponding author. Biology and Biotechnology Division, Lawrence Livermore National Laboratory, 7000 East Avenue, L-452, Livermore, CA 94550, USA.
E-mail address: loots1@llnl.gov (G.G. Loots).

Examination of SOST and its paralog, SOSTDC1 has revealed that these molecules can behave both as BMP (Kassai et al., 2005; Laurikkala et al., 2003; Winkler et al., 2003) and WNT antagonists (Ellies et al., 2006; Itasaki et al., 2003; van Bezooijen et al., 2004; van Bezooijen et al., 2007; Lin et al., 2009), generating some uncertainty about their molecular action, in vivo. Our previous work has described a transgenic mouse that overexpressses human SOST from a bacterial artificial chromosome, where elevated levels of SOST cause osteopenia; we also noted that these mice display limb defects. In the current study, we have investigated the role of SOST in limb patterning through genetic and molecular analyses of AER, ZPA, and limb-specific markers of BMP and WNT signaling pathways to understand the underlying mechanism of SOST action in the developing limb. In addition to evidence that SOST overexpression inhibits WNT/β-catenin signaling in vivo, we find that overexpression of SOST in $Sost^{tg};Lrp6^{+/-}$ mice modifies the otherwise phenotypically wild-type $Lrp6^{+/-}$ limb to mimic the Lrp6 knockout limb phenotype, while the removal of Sost in $Sost^{-/-};Lrp6^{-/-}$ double knockouts significantly rescues $Lrp6^{-/-}$ skeletal phenotypes, supporting a primary role for SOST in the inhibition of the WNT signaling pathway during the initial stages of limb bud formation, and a critical role for ectodermal-derived WNT signaling in the establishment of both the zone of polarizing activity and the apical ectodermal ridge.

Results and discussion

Characterization of limb defects in Sost gain-of-function embryos

We have previously reported that increased SOST expression in transgenic mice ($Sost^{tg}$) carrying a ~158 kb human BAC (Fig. 1A) led to low bone mass in the appendicular and axial skeleton (Loots et al., 2005). The observed osteopenia was shown to be gene dose-dependent, such that transgenic mice with higher levels of SOST exhibited a more dramatic decrease in tibial cancellous bone volume. $Sost^{tg}$ transgenics also displayed gene–dose-dependent limb abnormalities ranging from missing digits, fused, and split digits to loss of posterior bone structures (Loots et al., 2005; Fig. 1B and Fig. S1B and Fig. S2). In severely affected embryos, the limb bud appeared developmentally delayed and misshapen as early as E9.5, with truncation along the anterior-posterior axis (AP) axis, resulting in a cylindrical limb bud with reduced AER on the posterior side (Figs. 1c and d). By E12.5, we observed abnormal chondrocyte condensation of skeletal structures, and the formation of the phalanges was also delayed, with reduced separation or lack of digit formation. By E14.5, in most severely affected embryos, the ulna was absent, and digits 2 to 5 often failed to form (Fig. S1A).

Scoring of 117 neonates (77 $Sost^{tg}$ and 40 wild-type; derived from $Sost^{tg} \times Sost^{tg}$ and $Sost^{tg} \times$ wt matings) revealed that Sost gain-of-function most dramatically perturbs the autopod and zeugopod patterning along the A–P axis, where digit 5 (the most posterior autopod skeletal structure) was missing in 87% of $Sost^{tg}$ embryos. The ulna was absent from at least one forelimb in 22% of the $Sost^{tg}$ embryos, and 11% of $Sost^{tg}$ embryos completely lacked all autopod and zeugopod skeletal elements. The humerus and scapula were never affected, even in the most severe cases (Fig. 1B). We also observed a left–right asymmetry, such that the left forelimb and right hindlimb were more severely affected (Fig. S1B). To correlate the severity of digit abnormality with BAC copy number or zygosity, we examined human SOST expression in E11.5 limb buds derived from matings of phenotypically normal but hemizygous parents. Following Mendelian ratios, 25% of embryos were genotypically wild-type and 75% were $Sost^{tg}$. On average, one third of $Sost^{tg}$ limb buds were affected (resembling the embryo depicted in Fig. 1e, top panel) and the rest were phenotypically wild-type (resembling the embryo depicted in Fig. 1e, bottom panel). Using quantitative RT–PCR, we examined human SOST expression levels in pooled $Sost^{tg}$ embryos and found

100% of the affected embryos to have ~2× the amount of human SOST expression detected in phenotypically normal $Sost^{tg}$ embryos, confirming that the severity of limb defects correlates with Mendelian inheritance ratios, BAC zygosity, and human SOST expression levels (Fig. S2).

To examine whether human SOST was expressed according to the morphological changes in limb patterning, as well as whether it faithfully recapitulated the endogenous mouse Sost expression, we used in situ hybridization in wild-type or human SOST transgenic mice and β-galactosidase activity in mice where murine Sost has been replaced by LacZ. Supporting the validity of the LacZ expression, we found the knock-in expression to recapitulate mouse Sost expression monitored by in situ hybridization but with better signal-to-noise ratio (Figs. S3E, F); therefore, we used LacZ embryos to monitor mouse Sost expression. For both human and mouse Sost, we observed a dynamic pattern of expression that began during the initial stages of limb bud formation (~27-somite stage), where Sost was found to be expressed throughout the dorsal and ventral limb ectoderm (Figs. 1 and 2Q; Fig. S3). At E10.5, the expression was significantly higher on the ventral side, extended proximally to the trunk, while on the dorsal side, it was concentrated more distally, but excluded from the AER (Figs. 1d–f). This pattern continued until E12.5, when expression became distally restricted, although SOST expression continued to be excluded from the AER (Fig. 1f). Generally, murine and transgenic human SOST expression mirrored each other, with slight qualitative differences (Fig. S3), while quantitatively (using quantitative RT–PCR), we found endogenous mouse Sost expression to be 2-fold less than transgenic human SOST expression in defective embryos (Fig. S2).

To ensure the limb defects observed in $Sost^{tg}$ embryos result from high levels of SOST in its endogenous expression domain, rather than spatiotemporal misexpression of human SOST, we examined $Sost^{tg}$; $Sost^{-/-}$ embryos. We anticipated that limb defects resulting from an overdose will be fully or partially rescued by the lack of mouse Sost in $Sost^{-/-}$ embryos. All $Sost^{tg}$; $Sost^{-/-}$ embryos examined (N = 9) were fully rescued. Among $Sost^{tg}$; $Sost^{+/-}$ embryos 60% (N = 21) were fully normal and 40% (N = 14) had mild digit abnormalities (Table S1), suggesting that $Sost^{-/-}$ complements the limb defects caused by SOST overexpression in $Sost^{tg}$ transgenic embryos.

Repression of ZPA and AER genes in $Sost^{tg}$ limb buds

The loss of posterior skeletal elements observed in severely affected $Sost^{tg}$ animals (Fig. 1B) was highly reminiscent of two mutant strains: Wnt7A (Parr and McMahon, 1995) and Shh (Kraus et al., 2001) where digits 2–5 and the ulna were absent, while other proximal skeletal elements were unaffected. This suggested that elevated levels of SOST interfere either with establishing or maintaining the ZPA function to regulate digit formation and identity through the SHH morphogen (Ahn and Joyner, 2004; Kraus et al., 2001). Similar to limb buds deficient in Wnt7a, which is also expressed in the ectoderm, Shh expression was dramatically reduced in $Sost^{tg}$ limb buds (Figs. 2A–D). The decrease in Shh expression was variable from embryo to embryo, consistent with the range of loss of posterior skeletal elements observed in older animals (9/9 defective and 4/9 phenotypically normal $Sost^{tg}$ embryos showed reduced Shh limb expression by in situ hybridization). Despite ectodermal restriction of Sost expression and absence from the AER (Fig. 2Q; Fig. S3), AER gene expression was also affected in $Sost^{tg}$ and $Sost^{-/-}$ embryos. Both Fgf4 (Figs. 2E–H) and Fgf8 (Figs. 2I–L) were downregulated in $Sost^{tg}$ (11/11 defective and 7/13 normal $Sost^{tg}$ embryos showed reduced Fgf4 limb expression by in situ; 12/12 defective and 9/18 normal $Sost^{tg}$ embryos showed reduced Fgf8 limb expression by in situ). In particular, both Fgf-4 and -8 expression domains were narrower along the dorsoventral axis in $Sost^{tg}$ limb buds (Figs. 2F′ and J′, red arrow) and wider in $Sost^{-/-}$ limb buds (Figs. 2G′ and K′, green arrow), suggesting that Sost contributes to the establishment of the AER domain. While in situ
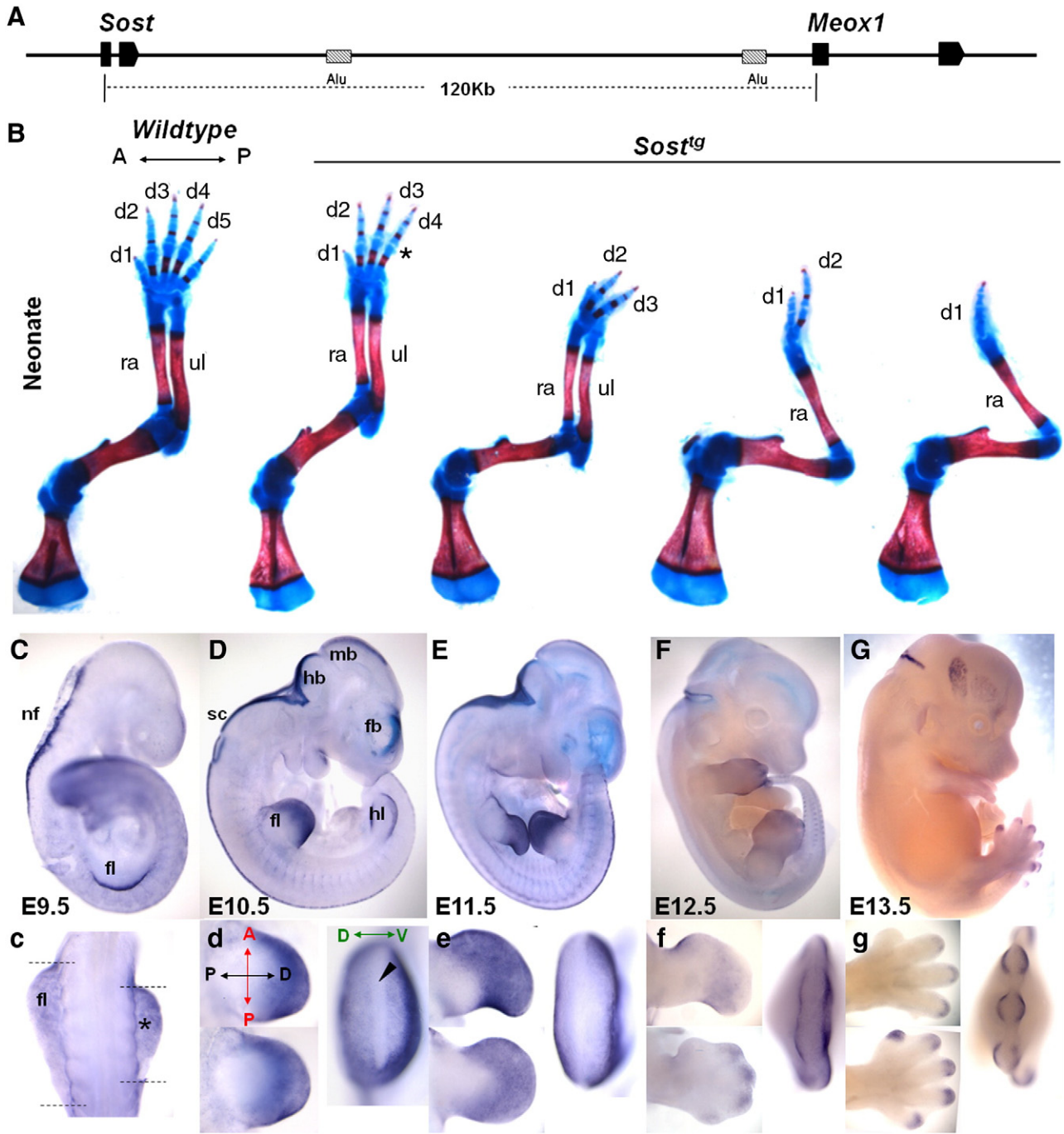
Fig. 1. Limb defects and human *Sost* expression in the *Sost^tg* developing limb. (A) A 158 kb human transgene spanning the *Sost* and *Meox1* transcript was used to generate the *Sost^tg* gain-of-function allele (Loots et al., 2005). (B) Skeletal preparations of E17.5 wild-type and *Sost^tg* embryos where *Sost* gain-of-function results in progressive loss of skeletal elements from posterior to anterior. A limb was scored as abnormal if it fell outside of the range observed in wild-type samples; 117 total animals were scored consisting of 77 *Sost^tg* and 40 wild-type (*d* digit, *ra* radius, *ul* ulna, *tg* transgenic, *wt* wild-type). (C–F) Human *Sost* expression was visualized by *in situ* hybridization using a human specific *Sost* probe, in a time course panel of E9.5 to E12.5 *Sost^tg* embryos. At each time point whole embryo (C–F), and dorsal limb and AER views are provided (c–f). Dorsal limb bud views are provided for two different *Sost^tg* littermate embryos at each time point, where the top limb corresponds to a severely affected embryos and the bottom limb is from a *Sost^tg* embryo that is morphologically indistinguishable from a wild-type limb bud. Asterisk highlights developmentally delayed mutant limb bud; arrowhead points to AER. *fl* forelimb, *hl* hindlimb, *nf* neural folds, *sc* spinal cord, *mb* midbrain, *fb* forebrain, *def* defective, *tg* transgenic.

hybridization revealed a dorsoventral expansion of the *Fgf8* domain in *Sost*^−/− embryos (Fig. 2K′), quantitative measurements (by quantitative RT–PCR) showed *Fgf8* mRNA to be also reduced in embryos lacking *Sost* (Fig. 2L), possibly due to loss of *Fgf8* expression in the anterior AER (Fig. 2K, black arrows). Despite the observed dorsoventral expansion, we attributed the decrease in *Fgf8* expression in *Sost*^−/− embryos to the weaker expression per cell and a more restricted anterior-posterior expression domain.

Although loss of *Shh* has been reported to result in decreased *Grem1* expression levels (Litingtung et al., 2002) at E10.5 (Fig. 2P), we found no quantitative change in *Grem1* expression in *Sost^tg* embryos. However, the *Grem1* expression domain expanded posteriorly into the region that lacks *Shh* positive cells (Figs. 2N and N′, red arrow), consistent with the observation that *Shh* descendants lack the ability to express *Grem1* (Scherz et al., 2004) (Figs. 2M–O). We also observed a strong shift in *Grem1* expression domain on the ventral side (the
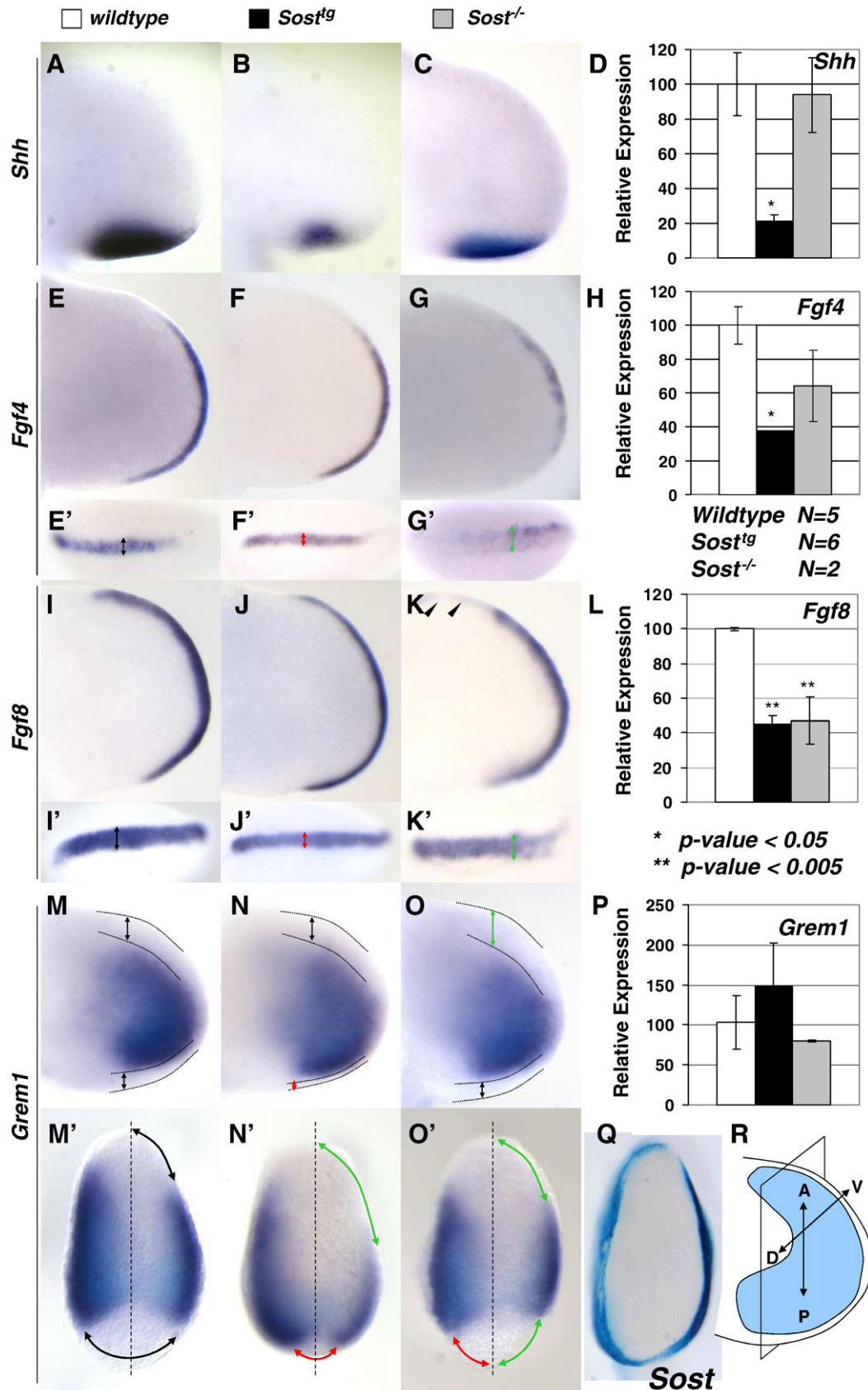
Fig. 2. Repression of ZPA and AER genes in *Sost*[tg]. (A–D) *Shh*, (E–H) *Fgf4*, and (I–L) *Fgf8* were significantly downregulated in *Sost*[tg] E10.5 limb buds. *Shh* was down to 20% its normal expression level in *Sost*[tg], but unaffected in *Sost*^{−/−} embryos (D). *Fgf4* and *Fgf8* were downregulated in both *Sost*[tg] and *Sost*^{−/−} embryos (H, L); the AER width was dependent on *Sost* levels, such that high levels of *Sost* limited its domain (J′, red arrow), while the absence of *Sost* disorganized and expanded it dorsoventrally (K′, green arrow). (M–P) *Grem1*, a mesenchymal marker, while quantitatively appeared unaffected (P), its expression domain (N, O) was altered in both gain- and loss-of-function embryos. In *Sost*[tg] embryos *Grem1* domain was expanded posteriorly (N′, red arrow), along with an anterior reduction on the ventral side (N′, green arrow). In *Sost*^{−/−} embryos similar asymmetric, but more subtle changes were observed (O′). (Q) Sost expression is restricted to the limb bud ectoderm. (R) Limb bud sections were carried out as illustrated.

dorsal side was unaffected) where *Sost* expression is the highest (Fig. 2Q), where in both *Sost^tg* (Fig. 2N′) and *Sost^{−/−}* (Fig. 2O′) embryos *Grem1* expression was excluded from the anterior region.

Genetic evidence of SOST as a WNT inhibitor

SOST was initially characterized as a BMP antagonist and, more recently, as a WNT antagonist. To determine if SOST favors the inhibition of BMP, WNT, or both of these pathways, in the limb, we examined genetic interactions between *Sost* gain- and loss-of-function alleles and *Grem1*, *Lrp5*, or *Lrp6* knockout alleles. The protein products of these genes are well- established components of the canonical BMP and WNT signaling pathways, respectively, and these mutants show limb defects of a similar nature to those observed in the *Sost* gain-of-function transgenic mice.

We reasoned that if secretion of SOST and GREM1 proteins primarily inhibit BMP signaling in the adjacent AER through epithelial–mesenchymal interactions (Michos et al., 2004; Panman et al., 2006), they may have redundant functions during limb patterning, such that elevated levels of *SOST* would potentially rescue the *Grem1^{−/−}* phenotype. Our rationale was based on the observation that both Noggin and Gremlin are BMP antagonists expressed in the limb bud which have the ability to interchangeably rescue gene expression changes in the limb bud of *ld* mutant mice (Khokha et al., 2003; Zuniga et al., 1999), yet their physiological roles in the limb bud are different, and their null phenotypes are distinctive (Brunet et al., 1998; Khokha et al., 2003; Zuniga et al., 1999). Alternatively, if *SOST* inhibits the canonical WNT pathway through one or both of the LRP receptors, elevated levels of *SOST* would modify the *Lrp5* and *Lrp6* limb knockout phenotypes. We found that elevated *SOST* expression fails to rescue but rather exacerbates the *Grem1^{−/−}* phenotype where 40% of *Sost^tg;Grem1^{−/−}* embryos (4 of 10) lack most autopod structures, and the zeugopod consists of a truncated bone fused to a dramatically shortened humerus (Fig. 3D and Table 1), indicating that *Sost* and *Grem1* are not acting in the same molecular pathway.

In contrast, we found that SOST shows strong interactions with the WNT pathway, consistent with SOST acting as a WNT inhibitor via its interactions with the WNT coreceptors LRP5 and LRP6 (Ellies et al., 2006; Itasaki et al., 2003; Li et al., 2005). Reduction of LRP function results in limb defects (Holmen et al., 2004) such that 35% of *Lrp5^{+/−};Lrp6^{+/−}* and 72% of *Lrp5^{−/−};Lrp6^{+/−}* are affected, where the severity follows the left to right and anterior–posterior axis, highly similar to *Sost^tg* phenotype (Figs. 1B and 3 and Table 1). Consistent with the idea that LRP6 is the more important receptor in the embryo, *Lrp6^{−/−}* mutants display strong effects in the limb, while *Lrp5^{−/−}* limbs develop normally. We found that *Sost^tg;Lrp6^{+/−}* mice have enhanced limb abnormalities closely resembling those of *Lrp6^{−/−}* limbs, relative to either *Lrp6* heterozygotes, which look phenotypically normal, or *Sost^tg* strain, suggesting that SOST inhibits LRP5/6 receptors (Fig. 3F). 20% of *Sost^tg;Lrp6^{+/−}* embryos also displayed spina bifida and tail truncation phenotypes similar to *Lrp6^{−/−}* homozygotes (Table 1; data not shown), suggesting that SOST also inhibits WNT signaling in the nervous system, consistent with *Sost* expression pattern (Figs. 1C–E). In addition, we observed a mild enhancement of the *Sost^tg* phenotype when LRP5 was reduced in *Sost^tg;Lrp5^{−/−}* embryos (Table 1) as further evidence that SOST interacts with both LRP5 and LRP6 coreceptors during limb development.

We also reasoned that elimination of the putative WNT antagonist SOST would elevate WNT signaling and rescue the limb phenotypes of *Lrp5/6* mutants. *Lrp6^{−/−}* forelimbs have a dramatically shortened zeugopod with one bone and two digits (Fig. 3E) while the hindlimbs lack the autopod and fibula and show fused hip bones (Fig. 3J). We found *Sost^{−/−};Lrp6^{−/−}* mice to have significantly rescued skeletons, where the forelimbs lack only digit 5 (Fig. 3H, compare to Fig. 3E). A more dramatic rescue was observed in the hindlimbs, where the absence of SOST resulted in hindlimbs that lack only 1–2 digits

(Fig. 3K), in contrast to the complete lack of autopods in *Lrp6^{−/−}* mice. Although reduced in size, the fibula was also restored in these animals, and the ilium bones were fully separated. *Lrp6^{−/−}* mice also have small heads, small eyes (microophthalmia), and cleft upper and lower lips, lack tails, and display different degrees of spina bifida (Pinson et al., 2000). The removal of SOST in *Sost^{−/−};Lrp6^{−/−}* mice ameliorated some of these defects (Fig. S4), but the most dramatic rescue was evident in the appendicular skeleton, where SOST rescued the hand and feet defects (Figs. 3H and K); this evidence demonstrates that SOST genetically interacts with the WNT signaling pathway during limb and skeletal development. Mechanistically, the loss of SOST, which normally interferes with WNT signaling, releases inhibition on other LRP receptors (possibly LRP5), allowing them to compensate for and partially rescue the complete loss of LRP6 receptor. In contrast, removing SOST in *Sost^{−/−};Grem1^{−/−}* double knockouts did not rescue *Grem1^{−/−}* autopod defects (data not shown).

Disruption of ectodermal and mesnchymal WNT signaling in the Sost^tg limb bud

To determine whether both *Sost^tg* and *Lrp6^{−/−}* limb defects may be mediated by the same direct or indirect molecular perturbations, we compared transcript levels in E10.5 forelimb buds of several key regulators thought to be involved in our model of WNT antagonism. We found levels of *Shh* and its target gene *dHand* to be ~20% and ~50% of normal expression in both *Sost^tg* and *Lrp6^{−/−}* limb buds (Figs. 4A and B). To determine whether both *Sost^tg* and *Lrp6^{−/−}* defective limbs both have reduced WNT signaling activity, we used quantitative RT–PCR to examine expression of Axin2, a direct target of Wnt/β-catenin signaling (Jho et al., 2002). *Axin2* transcript levels were significantly decreased in *Sost^tg* and *Lrp6^{−/−}* mutant limb buds (Fig. 4C), adding to the evidence that SOST inhibits the canonical WNT pathway in the limb.

Furthermore, we quantified transcript levels of 168 genes related to WNT and BMP function using quantitative RT–PCR arrays (Table S2). Nine genes were downregulated ≥ 1.5-fold in *Sost^tg* in each array, of which *Ctbp1*, *Jun* and *Wnt7A*, *Bmp2*, *Tgfbi* and *Bmp5* had significant *P* values. Inhibin alpha was the only gene upregulated in *Sost^tg* embryos, but no BMP-related transcripts were significantly upregulated in *Sost^{−/−}*. In contrast, while no WNT-related transcripts were elevated in *Sost^tg*, *Tcf3* transcription factor, a terminal component of the WNT signaling pathway that has been shown to function as a repressor (Cole et al., 2008), was significantly upregulated in *Sost^{−/−}*. The up-regulation of a repressor may explain the mild effect on downstream WNT targets, suggesting a protective autoregulatory mechanism for an overactive WNT pathway in the absence of *Sost* in the limb. *Tcf3* potentially curbs the overactive WNT signaling due to elevated levels of *Wnt5A* and *Wnt7A* transcripts and activated β-catenin protein detected by *in situ* and immunohisto-chemistry, respectively (data not shown).

To address how SOST interferes with WNT signaling regionally in the limb, we crossed the *SOST* gain-of-function transgene to the WNT reporter *BatGal* mouse (Maretto et al., 2003) and examined WNT responsiveness in the ectoderm, mesenchyme, and apical ectodermal ridge of the limb. At embryonic day 10.5, the *LacZ* stain of limb buds viewed in whole *BatGal* and *Sost^tg;BatGal* embryos initially looked indistinguishable and consistent with previously published limb patterns (Maretto et al., 2003), where the dominant expression of *LacZ* is in the AER (Figs. 5A and A′). Upon clearing, dissecting the limb buds and examining *LacZ* expression at higher magnification, and in sections, we observed a decrease in *LacZ*-positive cells in both the dorsal and ventral ectoderm and mesenchyme (Figs. 5B–F and B′–F′), within or immediately adjacent to the ectoderm that expresses the highest levels of SOST (Fig. 5G). These results suggest that ectodermal-derived SOST inhibits WNT signaling in both the ectoderm and the neighboring mesenchyme. β-Catenin is critical for
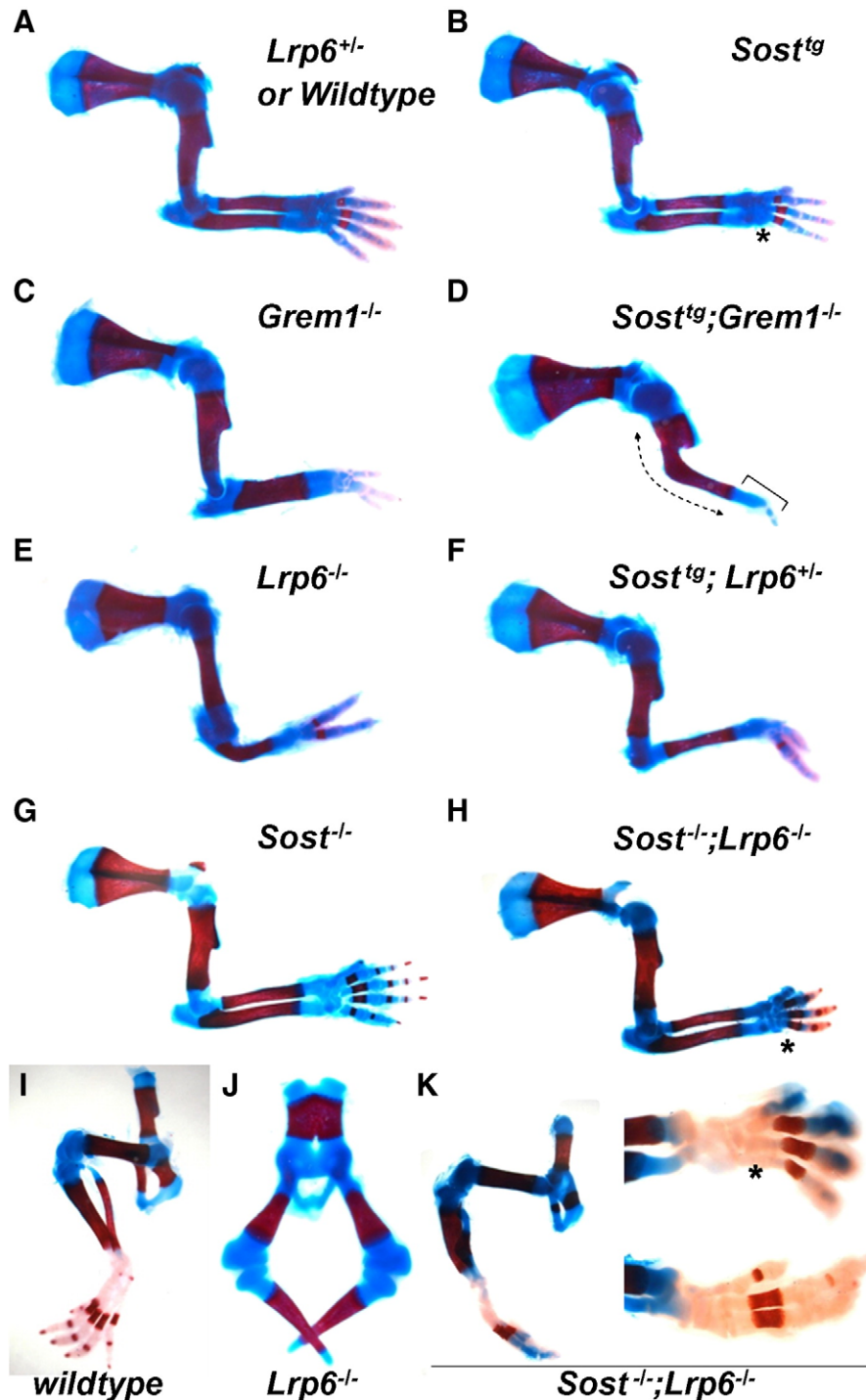
Fig. 3. *Sost* gain-of-function modifies both *Grem1*$^{-/-}$ and *Lrp6*$^{-/-}$ limb phenotypes, but *Sost* loss-of-function rescues only *Lrp6*$^{-/-}$. (A–H) Skeletal preparations of wild-type or *Lrp6*$^{+/-}$ (A), *Sost*^{tg} (B), *Grem1*$^{-/-}$ (C), *Sost*^{tg};*Grem1*$^{-/-}$ (D), *Lrp6*$^{-/-}$ (E), *Sost*^{tg};*Lrp6*$^{-/-}$ (F), *Sost*$^{-/-}$ (G), and *Sost*$^{-/-}$;*Lrp6*$^{-/-}$ (H) forelimbs. About 40% of *Sost*^{tg};*Grem1*$^{-/-}$ (D) forelimbs lacked an elbow, where the humerus, radius, and ulna have formed one skeletal element (arrow) and the wrist and autopod were highly reduced and lack most digits (bracket). While *Lrp6* heterozygous forelimbs were indistinguishable from wild-type, *Sost*^{tg} modified the *Lrp6* phenotype (E) such that *Sost*^{tg};*Lrp6*$^{+/-}$ forelimbs were indistinguishable from *Lrp6*$^{-/-}$ (F). Removal of *Sost* in the absence of *Lrp6* receptor resulted in dramatic rescue of *Lrp6*$^{-/-}$ limb phenotype (H). Most dramatic rescue of *Lrp6*$^{-/-}$ was observed in the hindlimbs (I,J), where lack of *Sost* restored hip morphology and autopod structure in *Lrp6*$^{-/-}$ mice (K). Digit 5 marked by an asterisk was never restored in autopods in *Sost*$^{-/-}$;*Lrp6*$^{-/-}$ mice (H, K).

transducing canonical WNT signals to the nucleus of responding cells, where it participates with Lef/Tcf transcription factors in the activation of downstream target genes (Behrens et al. 1996; Molenaar et al. 1996). It has been previously reported that the removal of β-catenin from the limb bud ectoderm results in severe limb defects characterized by lack of hindlimbs and severely truncated forelimbs (Barrow et al., 2003). These findings support the notion that ectodermal WNT signaling is required for proper AER function. While the *BatGal* mice are limiting in this regard, since they express *LacZ* at very low levels in the ectoderm, our results favor the conclusion that WNT signaling in both the ectoderm and the underling mesenchyme is abolished by SOST overexpression.

Table 1
Genetic analysis of Sost gain-of-function mutations in combination with mutations in members of the Wnt and Bmp signaling pathways.

Genotype	N	Forelimb	Hindlimb	Other
Sost^tg × Grem1^−/−				
Sost^tg	6	Normal	Normal	
	13	Loss of digits (3–4d rF, 3–5d lF)	Normal	
	1	Loss of digits (3d bF)	Loss of digits (1d lH)/Loss of fibula (lH)	
Grem1^+/−	17	Normal	Normal	
Grem1^−/−	10	Fused radius/ulna Loss of digits (3d bF)	Loss of fibula Loss of digits (0–3d bH)	
Sost^tg;Grem1^+/−	17	Normal	Normal	
	3	Loss of digits (2–4d rF, 3–5d rF)		
	6	Loss of digits (3–4d rF, 3–5d lF)	Loss of digits (3–4d lH)	
Sost^tg;Grem1^−/−	6	Fused radius/ulna Loss of digits (3d bF)	Loss of fibula/digits (0–3d bH)	
	4	Fused ulna/shortened humerus	Truncated tibia/no digits/Loss of fibula	
Sost^tg × Lrp5^−/−				
Sost^tg	14	Normal	Normal	
	16	Loss of digits (2–4d bF)	Normal	
	2	Loss of ulna/digits (2–3d bF)	Loss of digits (1d lH)/Loss of fibula	
Lrp5^+/− and Lrp5^−/−	31	Normal	Normal	
Sost^tg;Lrp5^+/−	21	Loss of digits (2–4d rF, 3–4d lF)	Normal	
	3	Loss of ulna/digits (2–4d bF)	Normal	Curly tail
Sost^tg;Lrp5^−/−	3	Loss of digits (4d rF)	Normal	
	5	Loss of digits (2–3d bf)	Loss of digits (3–5d bH)	Curly tail; runty; neonate death
Sost^tg × Lrp6^+/−				
Sost^tg	6	Normal	Normal	
	14	Loss of digits (2–4d bF)	Normal	
Lrp6^+/−	23	Normal	Normal	
Lrp6^−/−	11	Loss of ulna (lF)/short radius Loss of digits (4d rF, 2d lF)	Truncated femur/no digits	Spina bifida; no tail Abnormal/fused pelvis Cleft jaw/palate Microcephaly[a]; microopthalmia[a]
Sost^tg;Lrp6^+/−	25	Loss of digits—mild (2–5d bF, s lF) Dorsal ectopic nails	Loss of digits (3–5d bH) Dorsal ectopic nails	
	9	Loss of digits—severe (1–3d bF)	Truncated/no digits	Spina bifida Curly/truncated tail
Lrp5^−/− × Lrp6^+/−				
Lrp5^+/− and Lrp6^+/−	30	Normal	Normal	
Lrp5^+/−;Lrp6^+/−	19	Loss of digits (4d rF, small d5 lF)	Normal	
Lrp5^−/−;Lrp6^+/−	7	Loss of digits (2–3d bF)	Normal	
Sost^−/− × Lrp6^+/−				
Sost^+/− and Sost^−/−	27	Normal	Normal	
Lrp6^+/−	22	Normal	Normal	
Lrp6^−/−	11	Loss of ulna (lF)/short radius Loss of digits (4d rF, 2d lF)	Truncated femur/no fibula Lack of feet	Spina bifida, no tail Abnormal/fused pelvis Bilateral cleft jaw/palate Microcephaly[a]; microopthalmia[a]
Sost^+/−;Lrp6^+/−	18	Normal	Normal	
Sost^−/−;Lrp6^+/−	10	Normal	Normal	
Sost^−/−;Lrp6^−/−	8	Loss of digit (4d bF)	Loss of digits (3–4d bH) Loss of fibula (rH)	Spina bifida, no tail Unilateral cleft palate

d digit, F forelimb, H hindlimb, r right, l left, b both, s syndactyly.
[a] Rescue of phenotype was not quantified in Sost^−/−;Lrp6^−/−.

WNT signaling in the distal mesenchyme is required for anterior–posterior patterning

Our data show that elevated levels of SOST impair limb patterning along the A–P axis, where the most posterior digit 5 and the most posterior zeugopod element, the ulna, are often absent or abnormal in Sost^tg. We attribute these effects to excessive inhibition of WNT signaling, resulting in misregulation of genes in the two key limb centers, the zone of polarizing activity and the apical ectodermal ridge. Using the WNT signaling reporter BatGal, we were able to show that ectodermal expressed SOST suppresses WNT signaling both ventrally and dorsally, with the most dramatic down-regulation on the ventral side (where SOST is more highly expressed) where BatGal transgene signal is completely obliterated in the distal ectoderm and mesenchyme. On the dorsal side, BatGal transgene is expressed both in the proximal and distal mesenchyme (and in the ectoderm at very low levels), and consistent with SOST crescent moon expression pattern, BatGal transgene is repressed by SOST primarily in the distal region (mesenchyme and ectoderm). BatGal, as previously reported, is also expressed in the AER, region devoid of SOST expression, and in our gain-of-function allele, we observe an enhancement in LacZ AER expression (Figs. 5B′, D′, and F′, black arrow) when SOST is overexpressed in the neighboring ectoderm. Based on these changes in expression pattern of the WNT reporter, we can speculate that a net reduction in WNT signaling in the distal mesenchyme and ectoderm (both from the ventral and dorsal regions) results in an overall reduction of SHH expression level in the ZPA, suggesting that WNT signaling in distal mesenchyme/ectoderm is required for either establishing or maintaining SHH expression in the posterior mesenchyme of the developing limb. Since SHH turns on at E9.75, and most of our analysis was carried out at E10.5, we cannot differentiate between these two possibilities, nor can we determine if there is a delay in SHH activation. SHH has also been recently shown to be directly affected by β-catenin signaling, in that reduced β-catenin
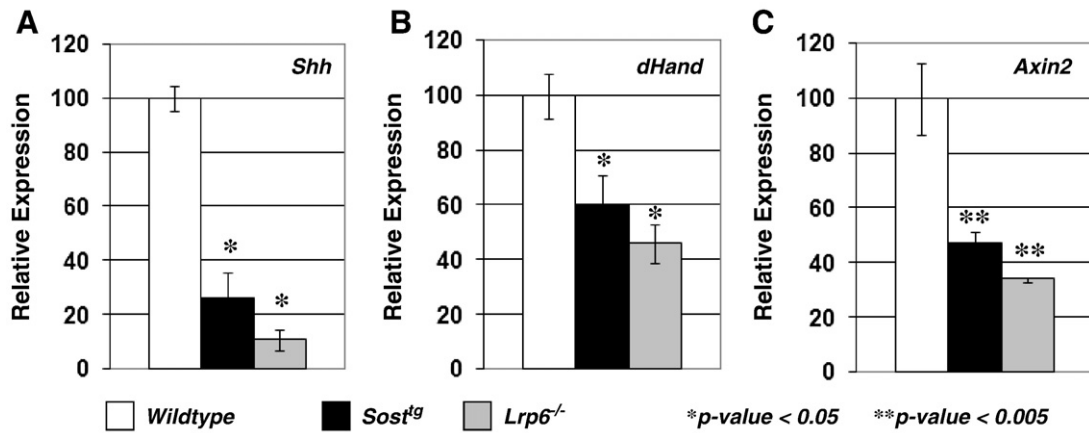
Fig. 4. Inhibition of *Shh* and WNT signaling in both *Sost^tg* and *Lrp6^−/−* limb buds. (A–C) Limb bud RNA was isolated from wild-type, *Sost^tg*, and *Lrp6^−/−* E10.5 limb buds. Normal expression of *Shh* (A) and its downstream transcriptional target *dHand* (B) was dramatically reduced in both *Sost^tg* and *Lrp6^−/−* embryos. Similarly, *Axin2* expression, a downstream target of canonical WNT signaling, was less than 50% of normal levels in both *Sost^tg* and *Lrp6^−/−* embryos (C).

signaling also directly reduces SHH expression (Miyagawa et al., 2009). Our findings are in support of WNT signaling acting upstream of SHH and positively regulating SHH transcription.

In parallel, we observed gene expression changes in the AER, where both *Fgf8* and *Fgf4* were found to be significantly repressed (Figs. 2E–L) in response to elevated levels of SOST. Since SOST is
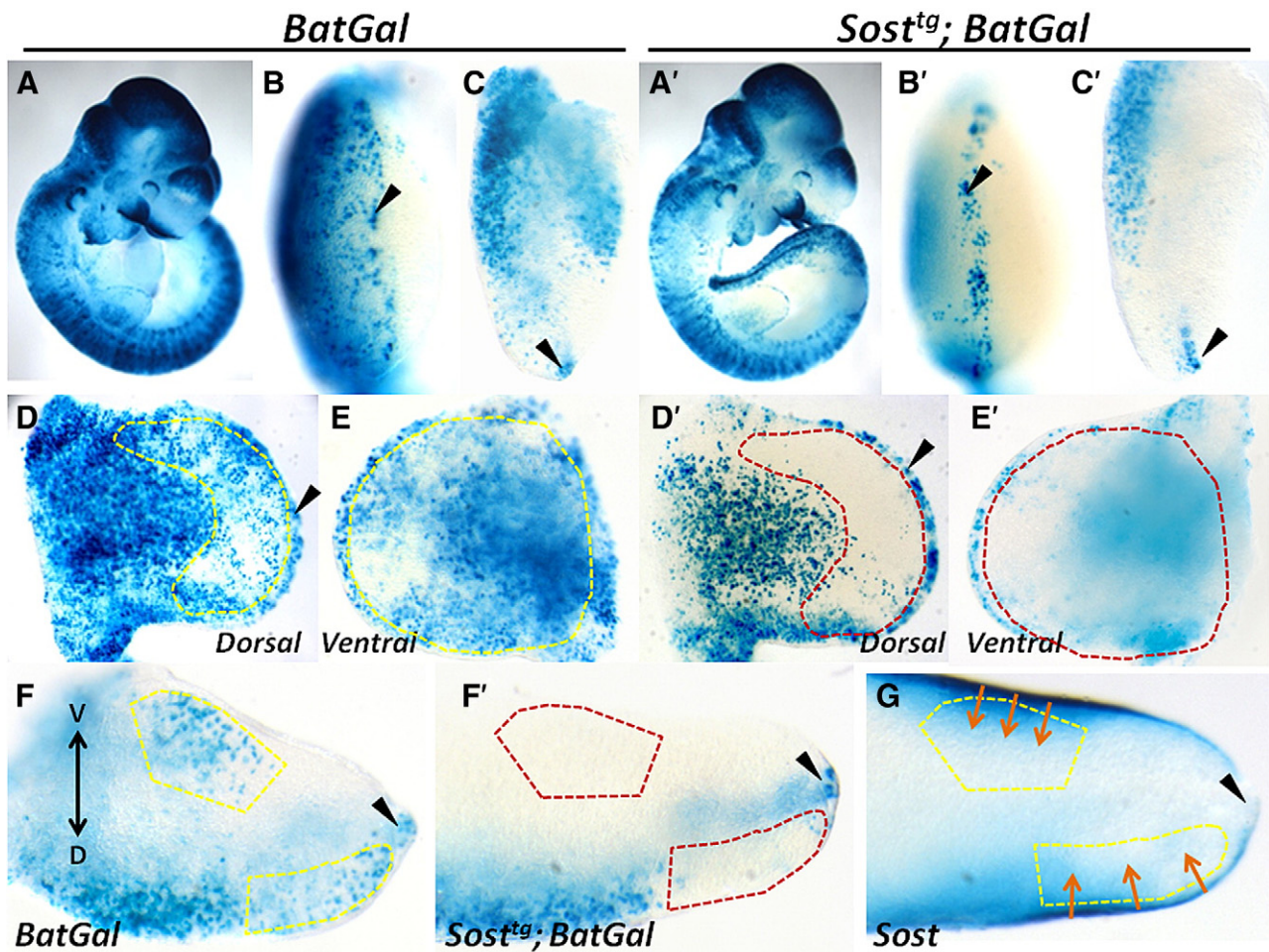

Fig. 5. Ectodermal SOST inhibits WNT signaling in the mesenchyme. (A–F) WNT activity in the limb was examined in *BatGal* WNT reporter mice. *LacZ* expression from the *BatGal* WNT reporter transgene was examined in E10.5 wild-type (A–F) and *Sost^tg* (A′–F′) embryos in whole mount (A and A′), AER limb views (B and B′), transverse limb sections (C, C′, F, and F′), dorsal (D and D′), and ventral (E and E′) limb bud views. Ectodermal-derived SOST (G) repressed *BatGal LacZ* reporter expression in the dorsal (D and D′) and ventral ectoderm (E and E′) in a pattern consistent with human *SOST* transgene expression (yellow dashed region). On the ventral side all reporter activity was lost (E′ and F′, red dashed region). AER *LacZ* expression was unaffected or enhanced in the presence of *SOST* (B′, D′, and F′). Black arrows indicate the AER, the region where *SOST* is absent (G), orange arrows indicate morphogenic activity of ectodermal-derived SOST to suppress WNT signaling in the underlining mesenchyme.

excluded from the AER, there are several alternate possibilities of how these molecular changes could have emerged. One possibility is that ectodermally expressed SOST inhibits ectodermal WNT signaling to interrupt the WNT3/β-catenin/FGF regulatory loop shown to be essential for AER establishment and maintenance (Barrow et al., 2003; Hill et al., 2006). The limb bud ectoderm represents a major source of WNT ligands (Witte et al., 2009); therefore, it is possible that SOST prevents WNT ligands such as WNT3 from binding to the LRP5/6 receptors within the ectoderm to attenuate WNT signaling in this tissue. Barrow et al. have shown that when they conditionally removed either *Wnt3* or β-catenin from the limb ectoderm using Msx2Cre, the mice display severe limb defects highly similar to both *Sost*[tg] and *Lrp6*^{−/−} limbs. In addition, Hill et al. observed that loss of mesenchymal β-catenin activity in the developing limb bud resulted in reduced expression of AER marker genes despite persistent β-catenin activity in the AER of the developing limb. While they reported severe limb truncations, we report varying degrees of posterior limb defects, and no distal truncations. This is likely due to the timing of and the extent of the loss of β-catenin activity, since in our model the loss of β-catenin /WNT signaling in the mesenchyme is incomplete, resulting in a less severe phenotype. While we observed very low levels of ectodermal *LacZ* expression in the *BatGal* mice, we cannot rule out that WNT signaling is not affected in the ectoderm, since our results are constrained by the restricted expression pattern of the *BatGal* transgene, which may not fully recapitulate the endogenous WNT activity.

Since limb development proceeds as a tightly coordinated series of morphogenic exchanges between various signaling centers, with very little cell autonomous activity, our results could also be explained as a modification of the ectoderm–ZPA–AER regulatory loop, where ectodermal and/or mesenchymal WNT signaling is required for SHH activity, and a dramatic reduction in SHH (we found SHH to be expressed at ~20% of normal levels in Sost[tg] and Lrp6^{−/−} limb buds; Fig. 4A) interferes with both ZPA and AER function. The proposed model of SOST action is similar and consistent with previously reported WNT signaling in the limb, whereby epithelial–mesenchymal interactions allow for transduction of signaling effects into neighboring tissues (ten Berge, et al., 2008). It has also been shown that SHH protein is present not only as a posterior gradient in the mesenchyme but also diffuses to the ectoderm and that posterior derived skin cells are derived from SHH-responsive cells (Gritli-Linde et al., 2001, Ahn and Joyner, 2004). Our results suggest that SOST is secreted by ectoderm and acts on the adjacent mesenchymal cells, a mode of action consistent with SOST's role during bone metabolism where osteocytes deeply buried in the bone secrete SOST, which travels to the surface of the bone where osteoblasts reside and inhibit their mineralization function (Balemans et al., 2001; Brunkow et al., 2001; Li et al., 2008a; van Bezooijen et al., 2004).

The changes in expression seen in *BatGal* and *Grem1* in the presence of the *SOST* transgene would suggest that there are dorsoventral patterning defects as well. No obvious dorsoventral mispatterning was observed in Sost[tg] mice. However, Sost[tg];Lrp6^{+/−} mice did display ventralization of the dorsal autopod in the form of ectopic nails on the dorsal surface, and Sost^{−/−} mice displayed ectopic pigment and hair on the ventral autopod (data not shown), suggesting dorsalization, which are consistent with perturbations in WNT signaling presented in Fig. 5.

Our findings are also consistent with recent reports that BMP signaling negatively regulates bone mass by induction of sclerostin which then inhibits the canonical WNT pathway (Kamiya et al., 2008). When Sost[tg] mice were crossed to *Grem1* mice which have limb defects as a direct result of overactive BMP signaling, SOST failed to compensate for the loss of *Grem1* and zeugopod and autopod formation was even further impaired. In contrast, when Sost[tg] mice were crossed to *Lrp5*^{+/−} and *Lrp6*^{+/−} mice, Sost[tg];Lrp6^{+/−} compound mice displayed defects that are more severe than those in *Lrp5*^{−/−};

Lrp6^{+/−} limbs, while the absence of *Sost* in *Sost*^{−/−};*Lrp6*^{−/−} limbs dramatically improves skeletal patterning, providing genetic evidence that *Sost* functions as a WNT antagonist during limb skeletogenesis. While our findings establish SOST as a WNT antagonist in the limb by these genetic criteria, we cannot rule out the possibility that SOST has some BMP-antagonistic activity, as previously suggested. One possible reason for the discrepancies between the previous data, where SOST was shown to inhibit the BMP pathway could be explained by a dual, context-dependent role of SOST, such that SOST affinity for one pathway is tissue-dependent.

Since WNT signaling is implicated in a multitude of processes and WNT ligands are broadly expressed spatially and temporally during vertebrate limb development, inhibitors of WNT signaling play an important role as gatekeepers of signal transduction and cell–cell communication across tissues. It is increasingly clear that a balanced combination of ligand expression and antagonistic regulation is required to ensure accurate WNT signaling and therefore proper limb outgrowth, patterning, and cartilage differentiation. Here we have shown that in addition to the pervasive high bone mass phenotype recorded for sclerosteosis patients and *Sost* knockout mice, SOST also contributes to the robustness of limb patterning signals by weakening the signal transduced through the LRP/6 receptors.

Materials and methods

Generation of compound mice

Sost[tg], *Grem1, Lrp5, Lrp6, BatGal*, and *Sost* mutant mice have been previously described (Holmen et al., 2004; Khokha et al., 2003; Li et al., 2008a; Loots et al., 2005; Maretto et al., 2003). *Sost* KOMP knockout mice were generated by a *LacZ* replacement of the entire *Sost* open reading frame. *Sost*[tg] or *Sost*^{−/−} mice were mated to *BatGal* individual knockout strains and the progeny were genotyped by PCR (primer sequences and PCR conditions available upon request). Progeny were selected for *Sost*[tg]; *BatGal*, Sost[tg];hets, or double hets and were mated to each other in timed matings; embryos were collected at E9.5, E10.5, E11.5, E12.5, E14.5, and/or E17.5, depending on the desired analysis, and the embryonic sac was genotyped by PCR. E0.5 of gestation was considered as noon on the day a visual copulatory plug was observed. Staging of embryos was verified where possible (before E12.5) by counting somites. All animal experiments were carried out in accordance with guidelines set by the Animal Care and Use Committee at University of California-Berkeley and Lawrence Livermore National Laboratory.

Whole-mount in situ hybridization

Whole-mount *in situ* hybridizations were carried out using standard procedures (Khokha et al., 2003). Species-specific sequences of human and mouse *Sost* were cloned from the 3′UTR region of each cDNA (human Sost NM_02537.2; mouse Sost NM_024449.4). Briefly, digoxigenin-labeled antisense RNA probes were generated to the desired RNA sequence and hybridized to whole-mount embryos. Expression was visualized by biding BM Purple (Roche). Antisense RNA probes for *Grem1* (*Mlu*I–*Sac*II fragment of NM_011824), *Fgf8* (PstI 3′ cDNA and UTR fragment of NM_010205; see Crossley and Martin, 1995), *Fgf4* (NM_01202.5), and *Shh* (*Msc*I–*Na*rI fragment of NM_009170; see Echelard et al., 1993) were generated as described (Hogan et al., 1994) with the following modification: proteinase K digestion was omitted for ectodermal or AER probes. A minimum of 4 embryos were used per genotype, per experiment. Wild-type controls were obtained from the same litter, whenever possible.

LacZ stains embryos

LacZ stains embryos were dissected free of extraembryonic membranes into ice-cold 1× phosphate-buffered saline (PBS), pH 7.3. Embryos were fixed in 2% paraformaldehyde, 0.2% glutaraldehyde in 1× PBS, 2 mM MgCl$_2$ at 4 °C for 30 minutes to 1 hour, followed by extensive rinsing in 1× PBS, 2 mM MgCl$_2$. Embryos were stained for 4 hours (*BatGal*) at RT or overnight (*Sost*$^{-/-}$) at 4 °C in X-gal stain: 1 mg/ml X-gal, 2 mM MgCl$_2$, 5 mM EGTA, 0.02% Nonidet P-40, 5 mM potassium ferrocyanide, 5 mM potassium ferricyanide, in 1× PBS, pH 7.3. After staining, embryos were postfixed in 4% paraformaldehyde in 1× PBS, pH 7.3 at 4 °C, and then cleared in glycerol for photography.

Skeletal preparations

Skeletal preparations were made of E17.5 day mouse embryos using Alcian Blue 8GX for cartilage and Alizarin Red S for bone following established protocols. Embryos were dissected free of internal organs, and skin, and fixed in 95% ethanol followed by stain in 0.05% Alcian Blue 8GX, 80% ethanol, 20% glacial acetic acid. Excess stain was washed out, and embryos were then stained in 60 mg/L Alizarin Red S, 1% potassium hydroxide (KOH), 25% glycerol followed by clearing in 1% KOH and 25% glycerol and storage in glycerol for photography. For skeletal preparation, whole litters were analyzed.

Quantitative RT–PCR

Total RNA was isolated from limb buds using Qiagen methods and reverse-transcribed into cDNA (Superscript II, Gibco). Quantitative RT–PCR expression analysis was performed using an ABI Prism 7900HT sequence detection system, TaqMan® Universal PCR Master mix, eukaryotic 18S rRNA predeveloped TaqMan® assay reagent for normalization and TaqMan® Assay-on-Demand™ products for mouse and human *Sost*, and murine *Fgf4*, *Fgf8*, *Shh*, *Grem1*, *dHand*, and *Axin2* (Applied Biosystems). For microarrays, 250 to 1000 ng of total RNA from E10.5 forelimbs was converted into cDNA using RT2 First Strand Kit (SA Biosciences), which included a genomic DNA elimination step.

Acknowledgments

Appendix A. Supplementary data

Supplementary data associated with this article can be found, in the online version, at doi:10.1016/j.ydbio.2010.03.021.

References

Ahn, S., Joyner, A.L., 2004. Dynamic changes in the response of cells to positive hedgehog signaling during mouse limb patterning. Cell 118, 505–516.

Balemans, W., Ebeling, M., Patel, N., Van Hul, E., Olson, P., Dioszegi, M., Lacza, C., Wuyts, W., Van Den Ende, J., Willems, P., Paes-Alves, A.F., Hill, S., Bueno, M., Ramos, F.J., Tacconi, P., Dikkers, F.G., Stratakis, C., Lindpaintner, K., Vickery, B., Foernzler, D., Van Hul, W., 2001. Increased bone density in sclerosteosis is due to the deficiency of a novel secreted protein (SOST). Hum. Mol. Genet. 10, 537–543.

Bandyopadhyay, A., Tsuji, K., Cox, K., Harfe, B.D., Rosen, V., Tabin, C.J., 2006. Genetic analysis of the roles of BMP2, BMP4, and BMP7 in limb patterning and skeletogenesis. PLoS Genet. 2, e216.

Barrow, J.R., Thomas, K.R., Boussadia-Zahui, O., Moore, R., Kemler, R., Capecchi, M.R., McMahon, A.P., 2003. Ectodermal Wnt3/beta-catenin signaling is required for the establishment and maintenance of the apical ectodermal ridge. Genes Dev. 17, 394–409.

Benazet, J.D., Bischofberger, M., Tiecke, E., Goncalves, A., Martin, J.F., Zuniga, A., Naef, F., Zeller, R., 2009. A self-regulatory system of interlinked signaling feedback loops controls mouse limb patterning. Science 323, 1050–1053.

Berge, D., Brugmann, S.A., Helms, J.A., Nusse, R., 2008. Wnt and FGF signals interact to coordinate growth with cell fate specification during limb development. Development 135, 3247–3257.

Behrens, J., von Kries, J.P., Bruhn, L., Wedlich, D., Grosschedl, R., Birchmeier, W., 1996. Functional interaction of beta-catenin with the transcription factor LEF-1. Nature 382, 638–642.

Brunet, L.J., McMahon, J.A., McMahon, A.P., Harland, R.M., 1998. Noggin, cartilage morphogenesis, and joint formation in the mammalian skeleton. Science 280, 1455–1457.

Brunkow, M.E., Gardner, J.C., Van Ness, J., Paeper, B.W., Kovacevich, B.R., Proll, S., Skonier, J.E., Zhao, L., Sabo, P.J., Fu, Y., Alisch, R.S., Gillett, L., Colbert, T., Tacconi, P., Galas, D., Hamersma, H., Beighton, P., Mulligan, J., 2001. Bone dysplasia sclerosteosis results from loss of the SOST gene product, a novel cystine knot-containing protein. Am. J. Hum. Genet. 68, 577–589.

Cole, M.F., Johnstone, S.E., Newman, J.J., Kagey, M.H., Young, R.A., 2008. Tcf3 is an integral component of the core regulatory circuitry of embryonic stem cells. Genes Dev. 22, 746–755.

Cremin, B.J., 1979. Sclerosteosis in children. Pediatr. Radiol. 8, 173–177.

Crossley, P.H., Martin, G.R., 1995. The mouse Fgf8 gene encodes a family of polypeptides and is expressed in regions that direct outgrowth and patterning in the developing embryo. Development 121, 439–451.

Duprez, D.M., Coltey, M., Amthor, H., Brickell, P.M., Tickle, C., 1996. Bone morphogenetic protein-2 (BMP-2) inhibits muscle development and promotes cartilage formation in chick limb bud cultures. Dev. Biol. 174, 448–452.

Echelard, Y., Epstein, D.J., St-Jacques, B., Shen, L., Mohler, J., McMahon, J.A., McMahon, A. P., 1993. Sonic hedgehog, a member of a family of putative signaling molecules, is implicated in the regulation of CNS polarity. Cell 75, 1417–1430.

Ellies, D.L., Viviano, B., McCarthy, J., Rey, J.P., Itasaki, N., Saunders, S., Krumlauf, R., 2006. Bone density ligand, Sclerostin, directly interacts with LRP5 but not LRP5G171V to modulate Wnt activity. J. Bone Miner. Res. 21, 1738–1749.

Galceran, J., Farinas, I., Depew, M.J., Clevers, H., Grosschedl, R., 1999. Wnt3a-/–like phenotype and limb deficiency in Lef1(−/−)Tcf1(−/−) mice. Genes Dev. 13, 709–717.

Gritli-Linde, A., Lewis, P., McMahon, A.P., Linde, A., 2001. The whereabouts of a morphogen: direct evidence for short- and graded long-range activity of hedgehog signaling peptides. Dev. Biol. 236, 364–386.

Hill, T.P., Taketo, M.M., Birchmeier, W., Hartmann, C., 2006. Multiple roles of mesenchymal β-catenin during murine limb patterning. Development 133, 1219–1229.

Hogan, B.L., Beddington, R., Costantini, F., Lacey, E., 1994. Manipulating the Mouse Embryo: A Laboratory Manual (2nd Edition). Cold Spring Harbor Press, New York.

Holmen, S.L., Giambernardi, T.A., Zylstra, C.R., Buckner-Berghuis, B.D., Resau, J.H., Hess, J. F., Glatt, V., Bouxsein, M.L., Ai, M., Warman, M.L., Williams, B.O., 2004. Decreased BMD and limb deformities in mice carrying mutations in both Lrp5 and Lrp6. J. Bone Miner. Res. 19, 2033–2040.

Itasaki, N., Jones, C.M., Mercurio, S., Rowe, A., Domingos, P.M., Smith, J.C., Krumlauf, R., 2003. Wise, a context-dependent activator and inhibitor of Wnt signalling. Development 130, 4295–4305.

Jho, E.H., Zhang, T., Domon, C., Joo, C.K., Freund, J.N., Costantini, F., 2002. Wnt/beta-catenin/Tcf signaling induces the transcription of Axin2, a negative regulator of the signaling pathway. Mol. Cell. Biol. 22, 1172–1183.

Kamiya, N., Ye, L., Kobayashi, T., Mochida, Y., Yamauchi, M., Kronenberg, H.M., Feng, J.Q., Mishina, Y., 2008. BMP signaling negatively regulates bone mass through sclerostin by inhibiting the canonical Wnt pathway. Development 135, 3801–3811.

Kassai, Y., Munne, P., Hotta, Y., Penttila, E., Kavanagh, K., Ohbayashi, N., Takada, S., Thesleff, I., Jernvall, J., Itoh, N., 2005. Regulation of mammalian tooth cusp patterning by ectodin. Science 309, 2067–2070.

Khokha, M.K., Hsu, D., Brunet, L.J., Dionne, M.S., Harland, R.M., 2003. Gremlin is the BMP antagonist required for maintenance of Shh and Fgf signals during limb patterning. Nat. Genet. 34, 303–307.

Kraus, P., Fraidenraich, D., Loomis, C.A., 2001. Some distal limb structures develop in mice lacking Sonic hedgehog signaling. Mech. Dev. 100, 45–58.

Laurikkala, J., Kassai, Y., Pakkasjarvi, L., Thesleff, I., Itoh, N., 2003. Identification of a secreted BMP antagonist, ectodin, integrating BMP, FGF, and SHH signals from the tooth enamel knot. Dev. Biol. 264, 91–105.

Li, X., Ominsky, M.S., Niu, Q.T., Sun, N., Daugherty, B., D'Agostin, D., Kurahara, C., Gao, Y., Cao, J., Gong, J., Asuncion, F., Barrero, M., Warmington, K., Dwyer, D., Stolina, M., Morony, S., Sarosi, I., Kostenuik, P.J., Lacey, D.L., Simonet, W.S., Ke, H.Z., Paszty, C., 2008a. Targeted deletion of the sclerostin gene in mice results in increased bone formation and bone strength*. J. Bone Miner. Res. 23, 860–869.

Li, X., Ominsky, M.S., Warmington, K.S., Morony, S., Gong, J., Cao, J., Gao, Y., Shalhoub, V., Tipton, B., Haldankar, R., Chen, Q., Winters, A., Boone, T., Geng, Z., Niu, Q.T., Ke, H.Z., Kostenuik, P.J., Simonet, W.S., Lacey, D.L., Paszty, C., 2008b. Sclerostin antibody treatment increases bone formation, bone mass and bone strength in a rat model of postmenopausal osteoporosis *. J. Bone Miner. Res. 24, 578–588.

Li, X., Zhang, Y., Kang, H., Liu, W., Liu, P., Zhang, J., Harris, S.E., Wu, D., 2005. Sclerostin binds to LRP5/6 and antagonizes canonical Wnt signaling. J. Biol. Chem. 280, 19883–19887.

Lin, C., Jiang, X., Dai, Z., Guo, X., Weng, T., Wang, J., Li, Y., Feng, G., He, L., 2009. Sclerostin mediates bone response to mechanical unloading through antagonizing Wnt/β-catenin signaling. J. Bone Miner. Res. 24, 1651–1661.

Litingtung, Y., Dahn, R.D., Li, Y., Fallon, J.F., Chiang, C., 2002. Shh and Gli3 are dispensable for limb skeleton formation but regulate digit number and identity. Nature 418, 979–983.

Loots, G.G., Kneissel, M., Keller, H., Baptist, M., Chang, J., Collette, N.M., Ovcharenko, D., Plajzer-Frick, I., Rubin, E.M., 2005. Genomic deletion of a long-range bone enhancer misregulates sclerostin in Van Buchem disease. Genome Res. 15, 928–935.

Macias, D., Ganan, Y., Sampath, T.K., Piedra, M.E., Ros, M.A., Hurle, J.M., 1997. Role of BMP-2 and OP-1 (BMP-7) in programmed cell death and skeletogenesis during chick limb development. Development 124, 1109–1117.

Maretto, S., Cordenonsi, M., Dupont, S., Braghetta, P., Broccoli, V., Hassan, A.B., Volpin, D., Bressan, G.M., Piccolo, S., 2003. Mapping Wnt/beta-catenin signaling during mouse development and in colorectal tumors. Proc. Natl. Acad. Sci. U. S. A. 100, 3299–3304.

Michos, O., Panman, L., Vintersten, K., Beier, K., Zeller, R., Zuniga, A., 2004. Gremlin-mediated BMP antagonism induces the epithelial-mesenchymal feedback signaling controlling metanephric kidney and limb organogenesis. Development 131, 3401–3410.

Miyagawa, S., Moon, A., Haraguchi, R., Inoue, C., Harada, M., Nakahara, C., Suzuki, K., Matsumaru, D., Kaneko, T., Matsuo, I., Yang, L., Taketo, M.M., Iguchi, T., Evans, S.M., Yamada, G., 2009. Dosage-dependent hedgehog signals integrated with Wnt/b-catenin signaling regulate external genitalia formation as an appendicular program. Development 136, 3969–3978.

Molenaar, M., van de Wetering, M., Oosterwegel, M., Peterson-Maduro, J., Godsave, S., Korinek, V., Roose, J., Destree, O., Clevers, H., 1996. XTcf-3 transcription factor mediates beta-catenin-induced axis formation in Xenopus embryos. Cell 86, 391–399.

Niehrs, C., 2006. Function and biological roles of the Dickkopf family of Wnt modulators. Oncogene 25, 7469–7481.

Niemann, S., Zhao, C., Pascu, F., Stahl, U., Aulepp, U., Niswander, L., Weber, J.L., Muller, U., 2004. Homozygous WNT3 mutation causes tetra-amelia in a large consanguineous family. Am. J. Hum. Genet. 74, 558–563.

Panman, L., Galli, A., Lagarde, N., Michos, O., Soete, G., Zuniga, A., Zeller, R., 2006. Differential regulation of gene expression in the digit forming area of the mouse limb bud by SHH and gremlin 1/FGF-mediated epithelial–mesenchymal signalling. Development 133, 3419–3428.

Parr, B.A., McMahon, A.P., 1995. Dorsalizing signal Wnt-7a required for normal polarity of D–V and A–P axes of mouse limb. Nature 374, 350–353.

Pinson, K.I., Brennan, J., Monkley, S., Avery, B.J., Skarnes, W.C., 2000. An LDL-receptor-related protein mediates Wnt signalling in mice. Nature 407, 535–538.

Pinzone, J.J., Hall, B.M., Thudi, N.K., Vonau, M., Qiang, Y.W., Rosol, T.J., Shaughnessy Jr., J.D., 2009. The role of Dickkopf-1 in bone development, homeostasis, and disease. Blood 113, 517–525.

Scherz, P.J., Harfe, B.D., McMahon, A.P., Tabin, C.J., 2004. The limb bud Shh–Fgf feedback loop is terminated by expansion of former ZPA cells. Science 305, 396–399.

Sutherland, M.K., Geoghegan, J.C., Yu, C., Turcott, E., Skonier, J.E., Winkler, D.G., Latham, J.A., 2004. Sclerostin promotes the apoptosis of human osteoblastic cells: a novel regulation of bone formation. Bone 35, 828–835.

van Bezooijen, R.L., Roelen, B.A., Visser, A., van der Wee-Pals, L., de Wilt, E., Karperien, M., Hamersma, H., Papapoulos, S.E., ten Dijke, P., Lowik, C.W., 2004. Sclerostin is an osteocyte-expressed negative regulator of bone formation, but not a classical BMP antagonist. J. Exp. Med. 199, 805–814.

van Bezooijen, R.L., Svensson, J.P., Eefting, D., Visser, A., van der Horst, G., Karperien, M., Quax, P.H., Vrieling, H., Papapoulos, S.E., ten Dijke, P., Lowik, C.W., 2007. Wnt but not BMP signaling is involved in the inhibitory action of sclerostin on BMP-stimulated bone formation. J. Bone Miner. Res. 22, 19–28.

Winkler, D.G., Sutherland, M.K., Geoghegan, J.C., Yu, C., Hayes, T., Skonier, J.E., Shpektor, D., Jonas, M., Kovacevich, B.R., Staehling-Hampton, K., Appleby, M., Brunkow, M.E., Latham, J.A., 2003. Osteocyte control of bone formation via sclerostin, a novel BMP antagonist. Embo J. 22, 6267–6276.

Witte, F., Dokas, J., Neuendorf, F., Mundlos, S., Stricker, S., 2009. Comprehensive expression analysis of all Wnt genes and their major secreted antagonists during mouse limb development and cartilage differentiation. Gene Expr. Patterns 9, 215–223.

Woods, C.G., Stricker, S., Seemann, P., Stern, R., Cox, J., Sherridan, E., Roberts, E., Springell, K., Scott, S., Karbani, G., Sharif, S.M., Toomes, C., Bond, J., Kumar, D., Al-Gazali, L., Mundlos, S., 2006. Mutations in WNT7A cause a range of limb malformations, including Fuhrmann syndrome and Al-Awadi/Raas-Rothschild/Schinzel phocomelia syndrome. Am. J. Hum. Genet. 79, 402–408.

Yanagita, M., 2005. BMP antagonists: their roles in development and involvement in pathophysiology. Cytokine Growth Factor Rev. 16, 309–317.

Zuniga, A., Haramis, A.P., McMahon, A.P., Zeller, R., 1999. Signal relay by BMP antagonism controls the SHH/FGF4 feedback loop in vertebrate limb buds. Nature 401, 598–602.